

DOTTORATO DI RICERCA IN
SCIENZE CLINICHE

CICLO XXXIV

COORDINATORE Prof. Lorenzo Cosmi

Characterization of Connective Tissue Disorders related Interstitial Lung Disease
(CTD-ILD)

with Computed Tomography (CT) and Magnetic Resonance Imaging (MRI)

Settore Scientifico Disciplinare MED/36

Dottorando

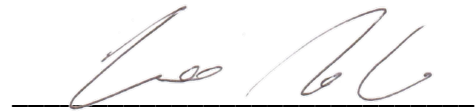
Dott. Nicholas Landini



(firma)

Tutore

Dott. Cosimo Nardi



(firma)

Coordinatore

Prof. Lorenzo Cosmi



Prof. COSMI LORENZO
Matr. 898314

(firma)

Anni 2018/2021

**Characterization of Connective Tissue Disease related Interstitial Lung
Diseases (CTD-ILD) with Computed Tomography (CT) and Magnetic
Resonance Imaging (MRI)**

SUMMARY

ABSTRACT.....	3
1. INTRODUCTION	5
1.1 Interstitial Lung Disease in Connective Tissue Disorders: definition, epidemiology, pathogenesis ...	5
1.2 Role of Computed Tomography in Interstitial Lung Disease related to Connective Tissue Disorders	6
1.3 Interstitial lung disease related to Connective Tissue Disorders: new frontiers of therapy and limits of CT	8
1.4 Magnetic Resonance imaging in Interstitial lung disease related to Connective Tissue Disorders: potential applications and purpose of the study.....	8
2. MATERIALS AND METHODS.....	14
2.1 Study design	14
2.2 Imaging systems and acquisition protocol.....	14
2.3 Image analysis	15
2.4 Statistical analysis	17
3. RESULTS.....	18
3.1 Patients cohort.....	18
3.2 ILD presence and extent and contrast evaluation	18
3.3 Observers Agreements	20
3.4 UTE-MRI performance	21
4. DISCUSSION	23
5. CONCLUSIONS	31

ABSTRACT

Purpose/Objectives

Interstitial Lung Disease (ILD) is a major complication of Systemic Sclerosis (SSc), with high morbidity and mortality. Computed tomography is the gold standard for ILD imaging assessment. However, recent Ultra-Short Echo-Time (UTE) Magnetic Resonance Imaging (MRI) sequences are promising for lung parenchyma evaluation. Moreover, different Dynamic Contrast Enhancement (DCE) MRI patterns seems able to identify prevalent inflammatory and fibrotic ILD, with possible implications in the management of the therapy. We aimed to verify the reliability of respiratory triggered UTE Spiral VIBE-MRI sequence in SSc-ILD assessment, compared to Computed Tomography (CT). Moreover, we tested the feasibility of DCE-MRI ILD analysis.

Materials and methods

54 SSc patients performed chest CT and MRI in the same day. The MRI protocol included a UTE Spiral VIBE sequence before contrast administration and a VIBE sequence, scanned pre and post contrast administration (after 1, 3, 5 and 10 minutes). Two radiologists, independently and in consensus, analyzed CT and UTE verifying ILD presence/absence and performing a semiquantitative analysis (sQA) of ILD, Ground Glass Opacities (GGO), Reticulations and Honeycombing (HC) extents on CT and UTE. A CT software quantitative texture analysis (QA) of alterations extents was also performed. Then, in patients with ILD on CT, the two readers assessed the prevalent CE pattern as following: pattern 1) early enhancement and washout with discernible peak enhancement at 1 or 3 min; pattern 2) slight enhancement with no discernible peak enhancement at a specific time-point; and pattern 3) delayed persistent enhancement with discernible peak enhancement at 5 or 10 min. Pattern 1 was considered inflammatory, patterns 2

and 3 fibrotic. For ILD detections as well as for DCE MRI analysis, intra- and inter-reader agreements were computed with Cohen's K coefficient. UTE sensitivity and specificity for ILD detection against CT were assessed. For extents analysis, intra-/inter-reader agreements and UTE performance against CT were computed by Lin's concordance coefficient (CCC).

Results

51 subjects were included for visual assessment, as 3 UTE were discarded for low quality. ILD was diagnosed in 39/51 CT. 16 out of the 51 included patients accepted to undergo VIBE pre and post contrast administration scans: 14 patients had ILD on CT and DCE-MRI were analyzed (no one discarded for low quality). UTE intra and inter-reader K in ILD diagnosis was 0.56 and 0.26, respectively. UTE showed 92.8% sensitivity and 75.0% specificity in ILD detection. 42 out of 51 QA segmentations were accepted. ILD, GGO and Reticulations extents were 14.8%, 7.7% and 7.1% on CT sQA and 13.0%, 11.2% and 1.6% on CT QA. HC was <1% and not further considered. UTE intra- and inter-reader CCC was 0.92 and 0.89 for ILD extent and 0.84 and 0.79 for GGO extent, respectively. UTE RET extent intra and inter-reader CCC was 0.22 and 0.18, respectively. ILD and GGO extents CCC were 0.95 and 0.93 against CT sQA and 0.89 and 0.88 against QA. RET extent CCC were 0.35 against CT sQA and 0.22 against CT QA. DCE-MRI analysis has intra- and inter-reader K of 1 and 0.63 (disagreement in one patient), respectively. Only one patient demonstrated a prevalent inflammatory pattern.

Conclusions

In SSc patients, UTE Spiral VIBE-MRI sequence may suffer of low inter-reader agreement in ILD detection, but it is a reliable tool in assessing ILD and GGO extents in ascertained ILD. DCE-MRI ILD evaluation seems feasible could add information on inflammatory ILD activity.

1. INTRODUCTION

1.1 Interstitial Lung Disease in Connective Tissue Disorders: definition, epidemiology, pathogenesis

Connective tissue disorders (CTD) are a heterogeneous group of diseases including rheumatoid arthritis (RA), systemic sclerosis (SSc), polymyositis / dermatomyositis (PM / DM), systemic lupus erythematosus (SLE), Sjögren's syndrome and mixed connective tissue disorders. Pulmonary involvement is a common complication of CTD and may affect various anatomical compartments of the lung: pleura, parenchyma, interstitium, vessels and airways may be interested, determining different manifestations of lung disease. Among these, Interstitial involvement is one the most frequent lung complication in CTD patients¹. The frequency of Interstitial lung disease (ILD) in CTD depends on subject selection and detection methods, but its prevalence seems to be higher than previously thought, leading to significant mortality. ILD may precede or follow the onset of rheumatic symptoms, and their early recognition is important, in order to start an appropriate therapy. The etiology of CTD-ILD is still unknown, and the current hypothesis regarding its pathogenesis are mainly based on data extrapolated from studies of SSc: inflammation triggered by external pathogens may cause the influx of inflammatory cells into the interstitial and alveolar spaces, giving rise to alveolar epithelial damage. The inflammation and epithelial damage lead to the recruitment and activation of lung fibroblasts and myofibroblasts, which produce increased amounts of extracellular matrix proteins and determine scarring within the lung. Pulmonary epithelial cells may also contribute to the pro-fibrotic mesenchymal cell population in lung fibrosis. Another hypothesis is that certain subtypes of CTDs begin with a lung-based process. It has been proposed that a lung injury triggering local inflammation induces auto-antigen expression, which can lead to the generation of autoantibodies in the lung. This may be perpetuated by the subsequent binding of disease associated autoantibodies and antigens, thus leading to further lung

inflammation and fibrosis.² Possible manifestation of Interstitial lung disease (ILD) are usual interstitial pneumonia (UIP), nonspecific interstitial pneumonia (NSIP), bronchiolitis obliterans organizing pneumonia (BOOP), diffuse alveolar damage (DAD) and lymphocytic interstitial pneumonia (LIP), identical to those of their idiopathic counterparts.³ Though there are variations in prevalence of histological patterns between the individual connective tissue disorders, NSIP is recognized as the most common pattern in CTD-ILD¹, particularly in SSc, PM/DM and mixed connective tissue disorders. In PM/DM BOOP is already common. On the other hand, UIP is the usual pattern in RA, while DAD in SLE and LIP in Sjögren's syndrome³.

1.2 Role of Computed Tomography in Interstitial Lung Disease related to Connective

Tissue Disorders

Chest computed tomography (CT), particularly high resolution computed tomography (HRCT), is currently considered to be the best clinically applicable modality for assessment of chest diseases in patients with CTD, permitting the evaluation of both individual patterns and extent of disease, as well as monitoring ILD⁴. NSIP features on CT are mostly sustained by ground-glass opacities and reticular abnormalities, associated to traction bronchiectasis or bronchiolectasis in fibrotic evolution. The involvement is predominantly in basal and peripheral. The parenchyma immediately adjacent to the pleura may be spared. Other findings such as consolidation and honeycomb cysts, are less common. Typical CT features of UIP are reticulations and honeycombing, with basal and peripheral distribution, frequently associated with traction bronchiectasis and bronchiolectasis. Ground- glass opacities may be seen, but they are usually less extensive than those in patients with NSIP. BOOP usually manifests as bilateral patchy areas of consolidation, often triangular or polygonal, in peripheral zones or in peribronchovascular regions, predominantly in the lower lung zones. Alterations may vary in dimensions tend to expand and migrate over time. Associated

ground-glass opacities are commonly associated, configuring the atoll sign or reverse halo sign⁵. IN UIP, ground-glass opacities are the dominant abnormality, and thin-walled perivascular cysts may be present. Lung nodules, reticulations, interlobular septal and bronchovascular thickening and widespread consolidation may also occur⁶. Lastly, DAD is often represented by bilateral ground-glass opacities with some sparing of individual lobules, producing a geographic appearance. In the organizing phase, architectural distortion, traction bronchiectasis, cysts, and reticular opacities may appear⁶.

On the other hand, the extents of ILD extent or main ILD alterations, such as ground glass opacities, reticulations and honeycombing, can be analyzed with both visual scoring methods and dedicated software, demonstrating also significant correlations with pulmonary function tests (PFT) ^{7,8}.

Furthermore, the extent of ILD detected on CT is recognized as a predictor of mortality⁹.

Most patients with CTD-ILD do not undergo a lung biopsy: it's now accepted that a UIP pattern on CT is virtually pathognomonic of underlying UIP at biopsy, while predominantly inflammatory histological patterns such as organizing pneumonia and lymphocytic interstitial pneumonia are generally associated with typical appearances on CT⁸. However, different patterns can be revealed in the same patient in histologic specimens, also in the same lobe^{10,11}. Thus, discriminating between UIP and NSIP on CT may be challenging. Moreover, ground glass opacities can reflect both inflammation and fibrosis on CT¹², making impossible to distinguish cellular from fibrotic NSIP in absence of architectural distortions. Ground glass opacities are increasingly considered early fibrosis in SSc patients, that may progress into defined reticulations and, eventually, towards clearly fibrotic alterations, depicted as architectural distortions, traction bronchiectasis and/or honeycombing¹³. However, in SSc patients treated with cyclophosphamide, ground glass opacities and reticulations revealed to be partially reversible. The reason that lies behind this observation remains unclear, but

it could account for different coexisting phenomena (fibrosis and inflammation) that can cause on CT same alteration¹⁴.

1.3 Interstitial lung disease related to Connective Tissue Disorders: new frontiers of therapy and limits of CT

Nowadays, the therapy of CTD-ILD mostly consists of corticosteroids and immunosuppressive therapy, since the control of inflammation is considered the main target². On the other hand, idiopathic pulmonary fibrosis (IPF), a purely primitive fibrotic ILD with a bad prognosis, deserve IPF antifibrotic drugs¹⁵. Thus, a correct and prompt diagnosis in patients with ILD is fundamental, in order to address the right management. However, also secondary ILD may rapidly evolve in fibrotic alterations and the term Progressive Fibrosis is taking field, irrespectively of classification and causes of fibrosis¹⁵. This concept has been leading to test antifibrotic drugs also in non-IPF with fibrotic ILD, with interesting results. The rationale that lies behind these studies is that all ILD that turn into fibrosis could benefit of drugs targeted on fibrogenesis suppression². From this perspective, the identification of fibrotic and inflammatory alterations may become pivotal and CT has some intrinsic limitation: being its evaluation predominantly morphologic, if clear signs of fibrosis, i.e. traction bronchiectasis, are absent, distinguishing between inflammatory or fibrotic ILD alterations, or mixed conditions, may be challenging¹⁶. On the other hand, Magnetic Resonance Imaging, could be able to identify inflammation and fibrosis irrespectively to the morphologic appearance of alterations¹⁷.

1.4 Magnetic Resonance imaging in Interstitial lung disease related to Connective Tissue Disorders: potential applications and purpose of the study

MRI has been considered as an oxymoron for many years. The main reason is that lung has a low proton density because it is 90% composed by air and the presence of air-water interfaces, forming

magnetic susceptibility gradients that cause rapid signal decay and image artifacts. Moreover, the cardio-respiratory movement determine numerous artifacts¹⁸.

However, recently developed MRI sequences, called ultra-short echo-time (UTE) sequences, are promising¹⁹. Ultra-short echo-time limits signal decay thanks to echo-time in the range of microseconds instead of milliseconds, providing high SNR and high-resolution images. Image quality of ultra-short echo-time has been described to be almost comparable to HRCT²⁰

Moreover, several functional MRI techniques might be complementary to CT in ILD.

Ventilation techniques with and without gaseous contrasts could provide important information regarding ventilation mismatch in ILD patients. The oxygen-enhanced MRI can be applied to assess regional ventilation, alveolar–capillary gas transfer of molecular oxygen, oxygen uptake per respiratory cycle and airflow limitation^{21,22}. This method uses the paramagnetic effect of pure oxygen to shorten T1 relaxation times, leading to a signal enhancement²³. Several studies have tested oxygen-enhanced MRI in patients with ILD. Molinari et al.²⁴ demonstrated a statistically significant correlation between oxygen-enhanced MRI and PFTs in patients with UIP (n=1), NSIP (n=8) and sarcoidosis (n=1). Ohno et al.²⁵ found that oxygen-enhanced MRI was comparable to HRCT to determine pulmonary functional loss and disease severity in ILD patients with CTD. Oxygen-enhanced MRI is a cheap and safe technique, but so far it has been performed in small groups of patients and in research settings, because it remains quite challenging with long scan acquisitions and poor SNR. Hyperpolarised gas-MRI, using helium (³He) or xenon (¹²⁹Xe) as gaseous contrasts provides quantitative regional information on pulmonary ventilation and lung microstructure changes. Currently, hyperpolarised gas-MRI has not been used in ILD and to date, no studies have been conducted in ILD with fluorinated gas MRI. Moreover, Stadler et al.²⁶ showed a shortening of the T1 relaxation time in patients with lung fibrosis, suggesting that T1 measurements could be used

to monitor disease progression and quantify the amount of lung fibrosis. Using T1 maps, Stadler et al.²⁷ investigated how the breathing status influenced T1 values of the lung parenchyma and demonstrated a statistically significant difference of inspiratory T1 values in comparison to expiratory ones both in healthy individual and patients with emphysema and fibrosis. Moreover, both pathological groups showed lower average T1 values in inspiration and expiration compared to healthy individuals while the average expiratory T1 was significantly higher in the fibrosis group than the emphysema group.

Active lung inflammatory tissue could be assessed with T2-weighted sequences or contrast-enhanced MRI. Lutterbey et al.²⁸ evaluated the feasibility of lung MRI at high magnetic field strengths (3.0T) using a fat suppressed (Fat-Sat) T2 Fast Spin Echo sequence to assess active versus non-active lung disease in ILD patients. This sequence is extremely sensitive to fluids. Since inflammation is accompanied by higher water content in the inflammatory tissue, they hypothesized a higher T2-weighted signal in active inflammatory lung lesions compared to chronic and fibrotic lung tissue. The results of their study showed that normal lung tissue appeared long T2 component signal free, that of fibrotic tissue was comparable to the muscle signal (intermediate signal), while inflammatory tissue showed high T2 (water-like) signal. Signal intensity was calculated by placing the region-of-interest in multiple lung areas with abnormalities and with different T2 signal intensity. HRCT was used as a reference standard to correlate morphological changes. Those lung areas with signal intensity twice higher that of the intermediate-signal areas were the lung area having the typical features of active ILD disease, such as GGO. These findings were also confirmed by pathological evaluation obtained on lung biopsy specimen. Similarly, Yi et al.²⁹ evaluated T2 intensity of ILD alterations in the area of the following biopsy, observing that a T2 intensity higher than paravertebral muscles may identify inflammatory components of ILD. Moreover, Buzan et al.³⁰, with T2 quantitative mapping, characterized and differentiated GGO, reticulation and HC in UIP and

NSIP. T2 sagittal maps were generated using a multi-echo single-shot, turbo spin echo sequence. Furthermore, they observed that T2 relaxation time tended to increase significantly with progression of fibrotic changes in ILD. On the other hand, T2 signal intensity proved to correlate with pulmonary function tests in patients with idiopathic pulmonary fibrosis³¹. Lastly, UTE sequences with a double echo acquisition should allow a quantification of the water content in lungs, that could be related to inflammatory activity in interstitial lung diseases. With regards to contrast-enhanced MRI, Yi et al.²⁹ studied the utility of 3.0T Dynamic Contrast Enhanced (DCE) MRI for differentiating inflammation and fibrosis predominant lesions in the UIP and NSIP, biopsy proven. DCE MRI consisted of T1-weighted three-dimensional turbo field-echo sequence using an intravenous bolus injection of gadopentetate dimeglumine. Enhancement pattern was visually assessed prospectively and classified into three categories using the dynamic contrast images: pattern 1) early enhancement and washout with discernible peak enhancement at 1 or 3 min; pattern 2) slight enhancement with no discernible enhancement at a specific time-point throughout dynamic phases; and pattern 3) delayed persistent enhancement with discernible peak enhancement at 5 or 10 min. Qualitatively analysis showed that 82% of inflammation-predominant lesions exhibited early enhancement (pattern 1) and that 94% of fibrosis-predominant lesions exhibited slight enhancement (pattern 2) or delayed persistent enhancement (pattern 3). The frequency of pattern 1 was significantly higher in the inflammation-predominant lung lesions (82% confidence interval). Quantitative assessment of dynamic enhanced MRIs were obtained by measuring the mean signal intensity of the lung lesions with regions-of-interest positioned by a radiologist in correlation to the HRCT findings. The following parameters were evaluated: maximum peak enhancement; time to peak; slope of enhancement; and extent of washout. Inflammation-predominant lesions sites had higher percentage signal intensity at 1 min, shorter time to peak and faster slope of enhancement than fibrosis- predominant sites. In summary, qualitative analysis of dynamic T1-weighted three-

dimensional turbo field-echo MRIs obtained at 3.0T proved helpful for differentiating inflammation- and fibrosis- predominant lesions. Gaeta et al.³² evaluated the gadolinium-enhanced MRI in the assessment of disease activity in 25 consecutive patients with chronic infiltrative lung diseases. They assumed that gadolinium enhancement might correlate with disease activity, because pulmonary insults inducing lung fibrosis disrupt capillary endothelium and permit the extravasation of contrast into the interstitial and alveolar spaces. Two radiologists retrospectively evaluated MRI and analyzed the studies for the presence (group 1) or absence (group 2) of pulmonary lesion enhancement. The presence of enhancement was considered predictive of active inflammation; the absence of enhancement was considered predictive of inactivity. The presence of enhanced pulmonary lesions was seen in 14 out of 17 patients with active disease. Negative enhancement was seen in all eight (100%) patients with inactive disease, and in three (18%) out of 17 patients with active disease. In both groups the difference was statistically significant (Fisher exact test, $p < 0.05$). These data showed that the presence of enhancing lesions on gadolinium-enhanced T1-weighted MRI studies may be a reliable indicator of inflammation and, consequently, potentially influence treatment choice and follow-up.

Lastly, the development of progressive parenchymal fibrosis in ILD patients causes lung restriction as a result of increased lung stiffness and reduced compliance. Recently, Marinelli et al.³³ investigated the use of magnetic resonance elastography in the quantitative assessment of pulmonary fibrosis by comparing quantitative shear stiffness measurements of lung parenchyma in patients with a diagnosis of ILD and normal controls. A 1.5 T two-dimensional spin-echo, echo planar imaging magnetic resonance elastography pulse sequence was utilized to assess absolute lung shear stiffness in 48 patients diagnosed with ILD and in 11 healthy controls. Lung shear stiffness was evaluated at residual volume and TLC. Prior to scanning all patients underwent spirometry. Patients with ILD exhibited an average shear stiffness of 2.74 kPa at TLC and 1.32 kPa at residual volume. The

corresponding values for healthy individuals were 1.33 kPa and 0.849 kPa, respectively. The difference in shear stiffness between residual volume and TLC was statistically significant ($p < 0.001$). This study demonstrated that the shear stiffness in patients with ILD, measured by magnetic resonance elastography, is increased when compared to healthy individuals at both residual volume and TLC. Because in this study the lung stiffness increases in ILDs with increasing transpulmonary pressure (i.e. from residual volume to TLC), the most significant difference in shear stiffness was demonstrated at TLC.

Given this background, we aimed to test reliability of a UTE MRI sequence (called Spiral VIBE) in ILD assessment, compared to CT, and to verify the feasibility of a DCE MRI analysis in patients with SSc.

2. MATERIALS AND METHODS

2.1 Study design

This was a prospective observational multicentric study (Departments of Radiology of AUOC Hospital, Florence, and Ca' Foncello General Hospital, Treviso). From February 2019 to February 2020, consecutive SSc patients referred to the rheumatologic dept. of AUOC (Florence), with suspected or ascertained ILD and in clinical need for a chest CT, were evaluated to undergo both chest CT and MRI examinations on the same day. SSc diagnosis was performed according the 2013 ACR/EULAR criteria³⁴. The exclusion criteria were: age < 18 years, heart failure or pulmonary disease other than ILD, contraindication to MRI, no inform consent, claustrophobia, impossibility lay supine for the scan time and/or to follow breathing instructions, low quality images for visual assessment or wrong software segmentation (see paragraph on *Image analysis*). Patients were referred to one of the two radiological centers based on geographical proximity and were instructed on how to perform the breathing manoeuvres. Recorded data included: age, gender, antibody subset, previous and ongoing therapy, pulmonary function tests (i.e. forced volume capacity, FVC, and diffusing capacity for carbon monoxide, DLCO) and presence of pulmonary arterial hypertension. The research project was approved by the local Institutional Ethics Committees: Careggi, Florence, protocol number 27299/2019, code 15220/oss and CESC Treviso and Belluno, protocol number 641/CECEAV.

2.2 Imaging systems and acquisition protocol

Chest CT scans were performed as follows: tube voltage 120 kV, tube current 200 mAs, slice thickness 1 mm, reconstruction kernels b35f and b60f and matrix 512x512. The CT scanners were a Sensation 64 and a Somatom Definition Flash (Siemens, Forchheim, Germany). Each CT acquisition took 3-5 seconds and was obtained at end of full inspiration, without contrast agent administration.

UTE-MRI scans were performed with two 1.5 T MRI systems (Aera and Avanto Fit; Siemens, Erlangen, Germany). The two MRI systems supported the same UTE sequence and the same parameters: Repetition Time 3.73 ms, Echo Time 0.05 ms, flip angle 5°, field of view 480x480, matrix 320x320 and voxel size 1.5x1.5x1.5 mm. UTE scans were free-breathing coronal acquisitions with a fully automated navigator trigger (Siemens-Dense), time of acquisition ranging 6-8 minutes. Images were reformatted in axial sections. No contrast agent was administered. An additional Volumetric Interpolated Breath-hold Examinations (VIBE) sequence were acquired before and after contrast administration (ProHance), at 1, 3, 5 and 10 minute after contrast injection. On both MRI scans the parameters were the following: Repetition Time 4.1 ms, Echo Time 1.57 ms, flip angle 9°, field of view 295x399, matrix 142x192 and voxel size 2.1x2.1x2.1 mm. The acquisition time was 14 seconds. All examinations were acquired with patients in supine position. Prone acquisitions, that might be performed to avoid the dependent atelectasis³⁵ were considered uncomfortable and inefficiently performable in a great percentage of our patients, given the MRI examination duration and patient clinical conditions.

2.3 Image analysis

CT and MRI scans quality was assessed in consensus by two chest radiologists of 10 and 12 years of experience in lung MRI (PC and GM). Scans were discarded as low quality images in presence of significant blurring of airways and/or peripheral lung parenchyma, as previously reported³⁶. Then, two thoracic radiologists with each 10 years of experience in thoracic imaging (NL and MO) evaluated CT and MRI scans. Firstly, they visually assessed the presence of ILD by the analysis of the whole parenchyma on CT and UTE. Then, they performed a visual semi-quantitative analysis (sQA) on both CT and UTE to compute the disease extent of lung ILD related abnormalities: GGO, RET and HC extents were scored as percentage of involved lung parenchyma (at the nearest 5%) at five

anatomical levels^{37,38}: 1) aortic arch, 2) carina, 3) confluence of pulmonary veins, 4) halfway between level 3 and 5, 5) immediately above right hemi-diaphragm. The ILD extent at each level was obtained summing the percentages of all abnormalities at that level. Then, the total GGO, RET, HC and ILD extents were computed as the mean percentage of the five levels. For instance, if GGO extent is 0%, 5%, 10%, 15%, and 20% for each of the five levels, the mean GGO extent was computed as $(0+5+10+15+20) / 5 = 10\%$ total lung parenchyma. Lung abnormalities were defined according to the radiological glossary of term the Fleischner Society⁶. GGO was defined as hazy increased opacity, with preservation of bronchial and vascular margins. RET was defined as a collection of innumerable small linear opacities that, by summation, produce an appearance resembling a net. HC was defined as clustered cystic air spaces that are usually sub-pleural, peripheral, and basal in distribution; the walls of the cysts are well-defined and often thick (1-3 mm). CT images were analyzed with high-resolution kernel, b60f, using a standard lung window, UTE window was visually adjusted to obtain the best contrast-to-noise ratio. CT and MRI scans were analyzed separately. Then, in patients with ILD on CT, VIBE Enhancement patterns were visually assessed and classified into three categories using DCE images, as previously reported²⁹: pattern 1) early enhancement and washout with discernible peak enhancement at 1 or 3 min; pattern 2) slight enhancement with no discernible peak enhancement at a specific time-point throughout dynamic phases; and pattern 3) delayed persistent enhancement with discernible peak enhancement at 5 or 10 min. Pattern 1 was considered inflammatory, patterns 2 and 3 fibrotic. Readers were asked to define the predominant pattern in ILD patients in terms of predominant inflammatory or predominant fibrotic. Readers assessed images independently and, after one month, one reader (NL) repeated the analysis. Lastly, both readers evaluated the images in consensus after an interval of 1 months. Discordances were discussed with a third senior radiologist (SC) with 30 years of experience in MRI imaging. In addition, an automated quantitative analysis (QA) of CT images was obtained on standard reconstruction

algorithms (b35f) by using Imbio Lung Texture Analysis software (Imbio LLC, Minneapolis, MN, USA) based on Computer Aided Lung Informatics for Pathology Evaluation and Rating (CALIPER) algorithm, as previously performed in SSc-ILD³⁸. The software segments the lung into 3 areas (upper, middle, and lower area), then identifies and quantifies percentages of GGO, RET, and HC. The total ILD score is computed as the sum of all abnormalities. One thoracic radiologist (MO) checked the software segmentations, ascertaining the inclusion of the whole lung parenchyma and the exclusion of other structures (i.e. trachea).

2.4 Statistical analysis

Cohen's Kappa test was used to compute intra/inter-reader agreement for SSc-ILD diagnosis on CT and UTE, as well as for DCE-MRI evaluation. Kappa values of 0.01–0.20, 0.21–0.40, 0.41–0.60, 0.61–0.80, 0.81–0.99 and 1 represented poor, fair, moderate, substantial, almost perfect and perfect agreement, respectively³⁹. Sensitivity, specificity, positive and negative predictive values⁴⁰ of UTE were computed. Lin's concordance correlation coefficient (CCC)⁴⁰ was used to compute intra-/inter-reader agreement for SSc-ILD extent analyses and to compare UTE consensus reading for disease extent analysis with CT, namely UTE sQA vs CT sQA and QA CT. The CCC values of 0.00–0.10, 0.11–0.40, 0.41–0.60, 0.61–0.80 and 0.81–1.0 represented no, slight, fair, good and very good agreement, respectively. Collected data were analyzed using the SPSS® v. 23.0 statistical analysis software (IBM Corp., New York, NY; formerly SPSS Inc., Chicago, IL).

3. RESULTS

3.1 Patients cohort

Seventy-six patients were initially screened by a rheumatologist (MaO) for CT and MRI examinations. 22 patients were excluded because of patient's refusal (n=6), MRI contraindication (n=7), claustrophobia (n=3), difficulty to perform respiratory maneuvers (n=3), and difficulty to maintain supine position (n=3). 38 patients refused the contrast administration. Therefore, 54 patients performed both CT and MRI scans on the same day. All 54 CT scans were considered adequate in terms of image quality. 3 UTE acquisitions were discarded because of poor image quality. Thus, 51 patients were included in the study for morphological evaluation. Furthermore, 9 CT QA were discarded because of wrong segmentations, thus 42 patients were considered to compare UTE to CT QA. 16/54 patients accepted to undergo VIBE acquisitions pre and post contrast administration. Demographical, serological, and clinical characteristics of patients are reported in Table 1.

3.2 ILD presence and extent and contrast evaluation

SSc-ILD was detected in 76.5% (39/51) on both CT and UTE sequences. The percentage of lung parenchyma affected by ILD, calculated as mean value of all patients, was 14.8% and 12.9% on CT sQA and UTE sQA, respectively. The mean ILD extent on 42 patients with available CT QA mean extents were 13.0% on CT QA and 12.8% on UTE sQA. All alterations extents are shown in Table 1. HC extent was found to be lower than 1% in all extent assessments and therefore considered irrelevant for further analysis. 14 out of 16 patients that underwent contrast administration had ILD. 1 of them (7%) demonstrated predominant areas of pattern 1, consistent with prevalent inflammatory ILD.

Table 1. Clinical, functional and radiological characteristics of the SSc population

CLINIC	CT sQA (n=51)	UTE (n=51)	p-value	CT QA (n=42)	UTE (n=42)	p-value
Age median (IQR)	50 (45-59)		-	49 (43-57)		-
Female (%)	43 (84)		-	38 (90)		-
SCL (%)	25 (61), n=41		-	22 (59), n=37		-
CENP-B (%)	13 (32), n=41		-	13 (35), n=37		-
FVC median (IQR)	92 (70-109)		-	91 (70-104)		-
DLCO median (IQR)	59 (41-69)		-	57 (40-68)		-
IS therapy (%)	26 (62), n=42		-	23 (62), n=37		-
Steroid therapy (%)	19 (45), n=42		-	18 (58), n=31		-
RADIOLOGY						
ILD-Extent mean % (SD)	14.8 (22.8)	12.9 (19.2)	>0.05	13.0 (19.7)	12.8 (19.9)	>0.05
GGO % (SD)	7.7 (15.2)	9.8 (17.4)	>0.05	11.2 (18.6)	9.7 (17.7)	>0.05
RET % (SD)	7.1 (10.0)	3.0 (4.6)	0.012	1.6 (1.8)	3.1 (4.6)	0.049
HC % (SD)	0.0 (0.2)	0 (0)	0.156	0.1 (0.3)	0 (0)	0.003

Legend

CT: computed tomography; sQA: semi-Quantitative Analysis in consensus reading; QA: Quantitative Analysis; UTE: Ultrashort Echo Time Spiral VIBE MRI sequence; ILD: Interstitial Lung Disease; GGO: Ground Glass Opacity; RET: Reticulation; HC: Honey Combing; SCL: anti-topoisomerase1 antibodies; CENP-B: anti-centromere B antibodies; FVC: Forced Vital Capacity; DLCO: Diffusion Lung Capacity

for carbon monoxide; IS: Immunosuppressive; IQR: Interquartile Range; SD: Standard Deviation; n: patients' number.

3.3 Observers Agreements

Intra-reader Cohen's kappa for ILD diagnosis showed almost perfect agreement for CT (k 0.95) and moderate agreement for UTE (k 0.56).

Intra-reader agreement for extent analyses was good to very good for total ILD, GGO, and RET on CT sQA (CCC ranging from 0.75 to 0.96). UTE sQA showed good to very good intra-reader agreement for ILD extent (CCC 0.92) and GGO extent (CCC 0.84), but poor for RET extent (CCC 0.22) (Table 2).

Inter-reader Cohen's kappa for ILD diagnosis showed substantial agreement (k 0.74) for CT and fair agreement for UTE (k 0.26). Inter-reader agreements for alterations extents was good to very good (CCC ranging from 0.76 to 0.94) for total SSc-ILD, GGO, and RET on CT sQA. UTE sQA showed very good inter-reader agreement for ILD extent (CCC 0.89) and good agreement for GGO extent (CCC 0.79), but poor inter-reader agreement for RET (CCC 0.18) (Table 2). Cohen's kappa for intra-reader and inter-reader agreement in dynamic contrast evaluation was 1 and 0.63 (disagreement in one patient), respectively.

Table 2. Intra-reader and inter-reader and agreement in semiquantitative extent analysis of total ILD and ILD related abnormalities, expressed by Lin's Concordance Correlation Coefficients (95% Confidence Interval).

INTRA-READER AGREEMENT	CT sQA	UTE
ILD	0.95 (0.94 - 0.96)	0.92 (0.89 - 0.95)
GGO	0.96 (0.95 - 0.97)	0.84 (0.81 - 0.87)
RET	0.75 (0.75 - 0.77)	0.22 (0.18 - 0.25)
INTER-READER AGREEMENT		
ILD	0.94 (0.94 - 0.94)	0.89 (0.89 - 0.90)
GGO	0.92 (0.92 - 0.93)	0.79 (0.78 - 0.80)
RET	0.76 (0.75 - 0.78)	0.18 (0.16 - 0.20)

Legend

CT: computed tomography; sQA: semi-Quantitative Analysis; UTE: Ultrashort Echo Time Spiral VIBE MRI sequence; ILD: interstitial lung disease; GGO: Ground Glass Opacity; RET: Reticulations

3.4 UTE-MRI performance

UTE sensitivity, specificity, positive and negative predictive values (confidence interval) in identifying SSc-ILD on consensus reading were 92.3% (79.1%-98.4%), 75.0% (42.8%-94.5%), 92.3% (79.1%-98.4%) and 75.0% (42.8%-94.5%). In particular, UTE generated 3 false negatives, with ILD extent on CT sQA of 1%, 3% and 3%, and 3 false positives, with computed ILD extent on UTE of 5%, 6% and 8%. The alterations extent analysis CCC between UTE and CT (sQA and QA, respectively) was

very good for total ILD (0.95 and 0.89) and GGO extent (0.93 and 0.88), whereas it was poor for RET extent (0.35 and 0.22) (Table 3).

Table 3. Lin's Concordance Correlation Coefficient between UTE and CT for ILD, GGO and RET extents (95% Confidence Interval)

	UTE vs CT sQA	UTE vs CT QA
ILD	0.95 (0.94 - 0.95)	0.89 (0.88 - 0.90)
GGO	0.93 (0.93 - 0.94)	0.88 (0.87 - 0.88)
RET	0.35 (0.34 - 0.36)	0.22 (0.21 - 0.23)

Legend

CT: computed tomography; UTE: Ultrashort Echo Time Spiral VIBE MRI sequence; sQA: semi-Quantitative Analysis as obtained by consensus reading; QA: CT Quantitative Analysis; ILD: Interstitial Lung Disease; GGO: Ground Glass Opacity; RET: Reticulation.

4. DISCUSSION

We tested the performance of UTE Spiral VIBE in the detection of SSc-ILD and in the assessment of disease extent, using CT as the reference standard. UTE Spiral VIBE proved to be reliable in ILD and GGO extent analysis (Figure 1 and 2). Thus, in our series the potential benefits deriving from new chest MRI techniques, as reported in state-of-art reviews^{17,42}, are confirmed.

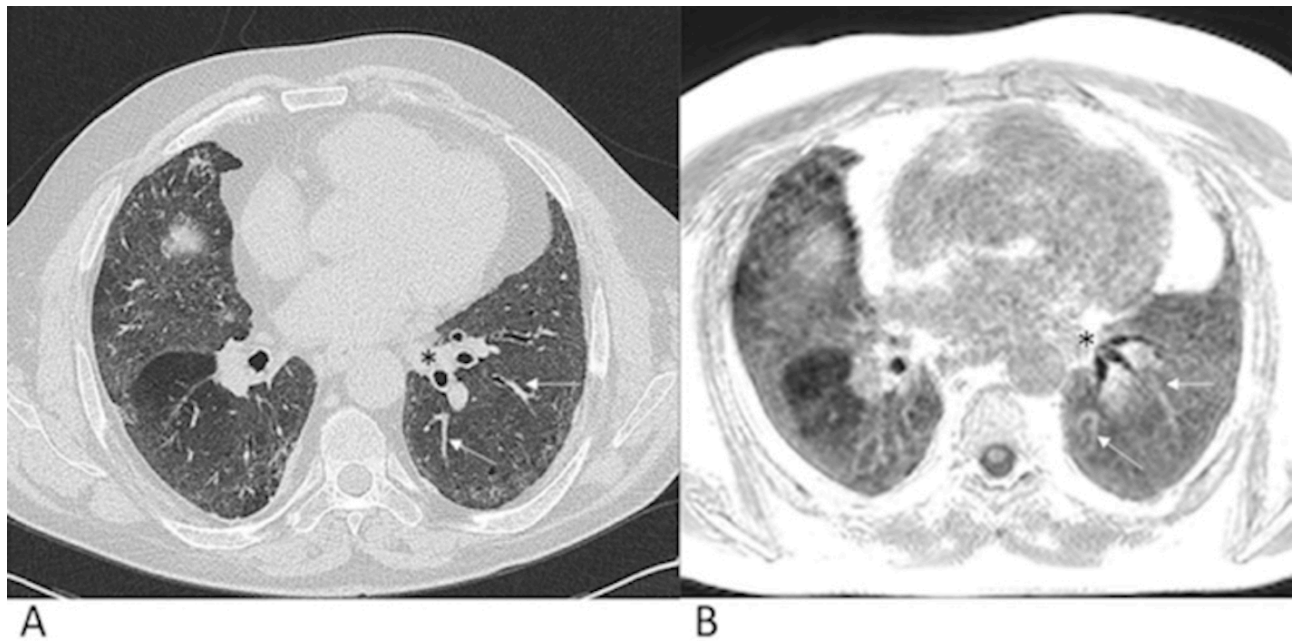


Fig. 1. CT and UTE sQA SSc-ILD extent analyses.

ILD was scored as 85% total lung parenchyma at level 5 on both CT (A) and UTE (B). Breath-hold CT and free-breathing UTE acquisitions may lead to slightly anatomical differences at the same level, as it was showed by left lower lobe bronchi (black asterisks): however, visualized segmental vessels are the same (white arrows).

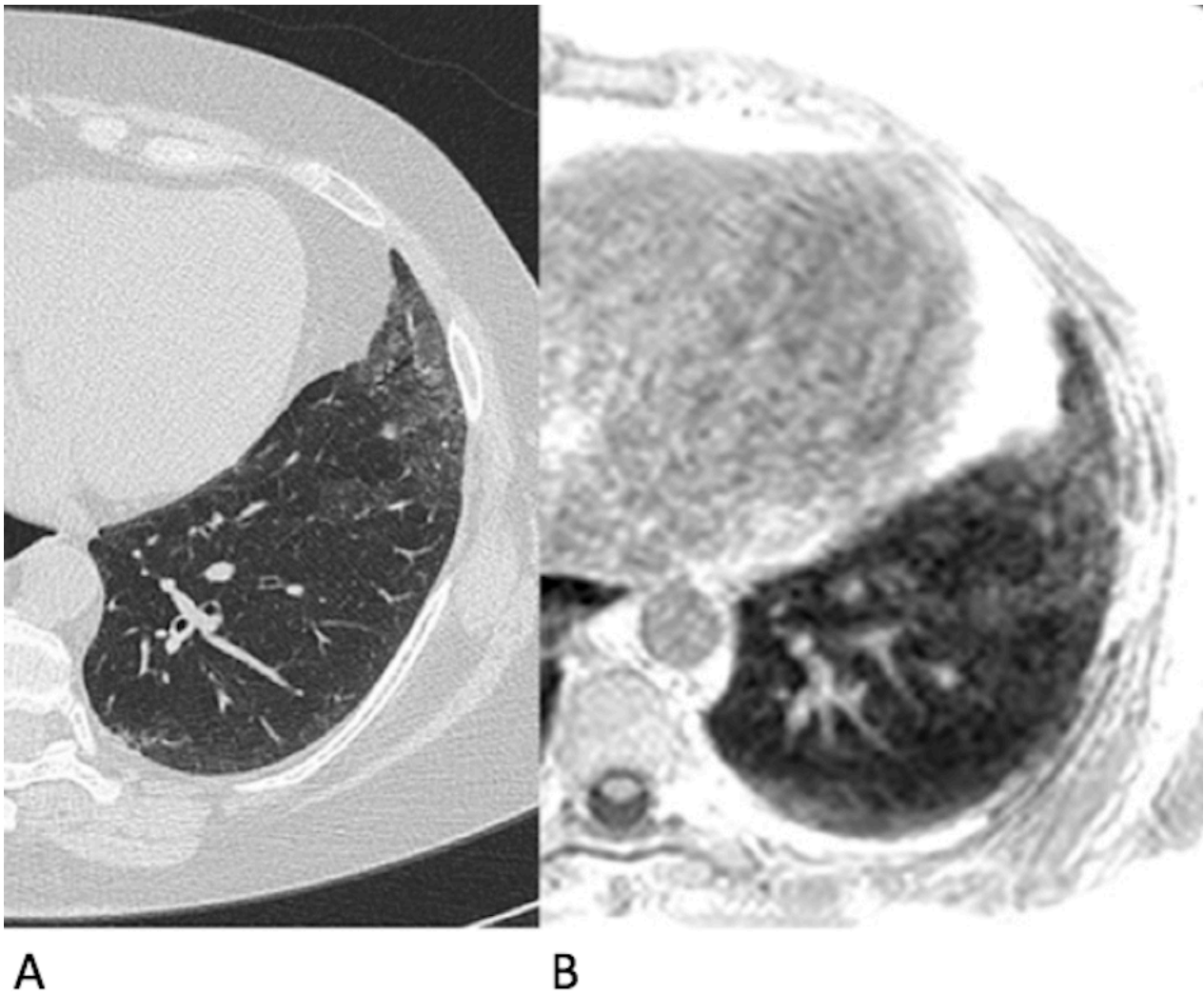


Fig. 2. SSc-ILD, left lung: ground glass opacities on CT and UTE.

CT areas of ground glass opacities (A) may be easily recognized and quantified on UTE (B)

Legend

SSc: Systemic Sclerosis; ILD: Interstitial Lung Disease; CT: Computed Tomography; GGO: ground glass opacity

UTE: Ultrashort Echo Time Spiral VIBE MRI sequence

The first paper that investigated the use of UTE in ILD extent assessment on SSc patients⁴³ used a 2D BH half-Fourier single-shot TSE sequence. This 2D sequence showed high sensitivity to detect SSc-ILD, but it was less reliable in evaluating disease extent. Generally, UTE sequences help to overcome the technical limits of MRI in the lung study by enabling both high signal-to-noise ratio

and high-resolution 3D lung morphological imaging. In fact, UTE sequences reduce the minimum time needed to cover k-space using a non-selective RF pulse. In particular, standard Cartesian phase encoding and Spiral sampling in-plane encoding is performed in UTE Spiral VIBE studied by us⁴⁴. Previous studies found good agreement of UTE sequences with CT in ILD detection^{44,45}, but none of these assessed the ability to quantify disease extent. The current study is the first one, as far as we know, that demonstrated the agreement between UTE sequences and CT in SSc-ILD extent evaluation.

Moreover, UTE Spiral VIBE acquisitions did not exceed 8 minutes' duration in our study and only 5% of them (3/54) were discarded for motion artefacts. This was a relevant result, as short scan time is pivotal in dyspneic patients, such those with SSc-ILD⁴⁶. Our Spiral VIBE exploits an improved automated respiratory gating that should make the scan more robust against motion artefacts than a previous zero-TE version, namely PETRA (Pointwise-Encoding-Time-Reduction-Radial-Acquisition). In fact, PETRA relies on navigator positioning with possible steady state interruption and longer acquisition time, depending on required resolution and actual breathing pattern of patients⁴⁴.

We also observed high sensibility and positive predictive value of UTE in ILD diagnosis, but intra/inter-reader agreements were lower than CT, for such task. As a matter of fact, especially in mild or no ILD, the assessment of lung parenchyma in expiration could have artificially increased the detection of GGO. The lung parenchyma in expiration has higher signal for partial collapse (atelectasis), especially in the dependent peripheral lung regions, that may be also the zones primarily affected by SSc-ILD¹³. This could justify the readers' discrepancy, since dependent GGO due to mild interstitial disease may be misinterpreted as partial alveolar collapse (atelectasis) and *vice versa*, as well as it is reasonably the issue that lies behind UTE false negatives and false positives against CT (Figure 3).

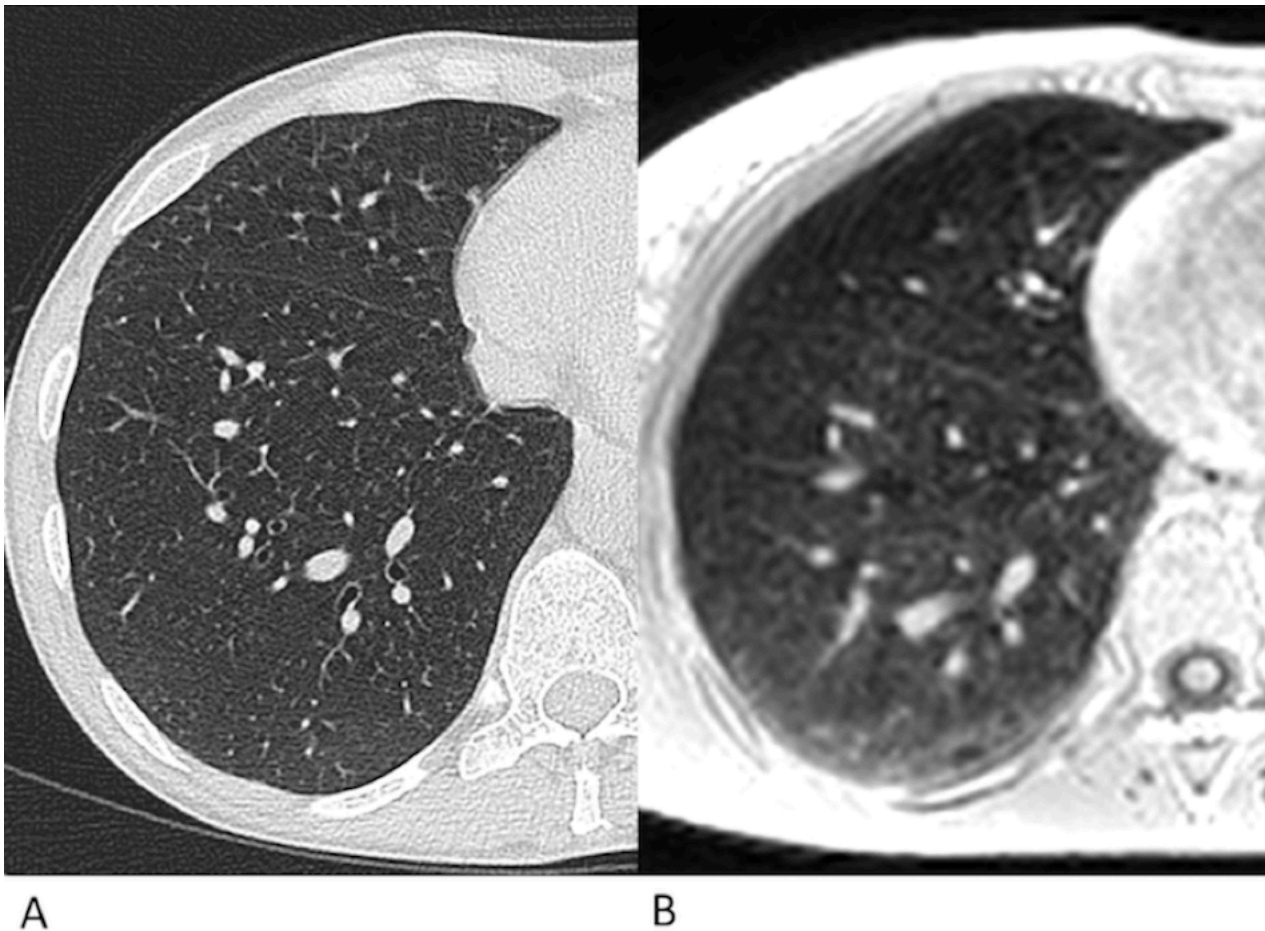


Fig. 3 SSc-ILD, right lung: false positive of ILD diagnosis on UTE.

CT (A) shows absence of ILD, but dependent atelectasis on UTE (B) may be interpreted as ground glass opacities due to ILD.

Legend

SSc: Systemic Sclerosis; CT: Computed Tomography; UTE: Ultrashort Echo Time Spiral VIBE MRI sequence; ILD: Interstitial Lung Disease

To overcome this problem, UTE could be acquired at full inspiration as recently shown by Veldhoen et al.⁴⁷. They achieved the best spatial and temporal resolution compromise with a breath-hold UTE of 2.3 mm (isotropic voxel) for a mean scan time of 115 seconds obtained with 5 breath-holds to cover the entire thorax. However, the setting proposed by Veldhoen et al.⁴⁷ requires a significant effort to the patient providing anyhow a spatial resolution lower than CT, since inspiration and small

voxel size could reduce lung signal affecting ILD evaluation. Nevertheless, considering the good performance in quantifying ILD and GGO extent, UTE could be now tested to monitor disease progression, especially in young patients with ascertained ILD and GGO as the predominant feature. In the clinical setting, a good policy to improve UTE diagnostic accuracy could be to acquire a baseline MRI scan at the same time of CT. Then, in selected subjects, MRI could be alternated to CT, adapting an imaging scheme adopted for other chronic lung diseases, such as cystic fibrosis⁴⁸. However, further studies are needed to confirm this hypothesis.

On the other hand, RET analysis in UTE sequences was scarcely reliable. Air-filled alveoli tend to reduce lung signal¹⁵ and might make the identification of thickened septa very challenging. Moreover, adjacent or superimposed areas GGO, due to ILD or partial alveolar collapse, could partially hide septal thickening (figure 4). Thus, the assessment of fine RET extent remains a limitation of chest MRI, even with UTE sequences.

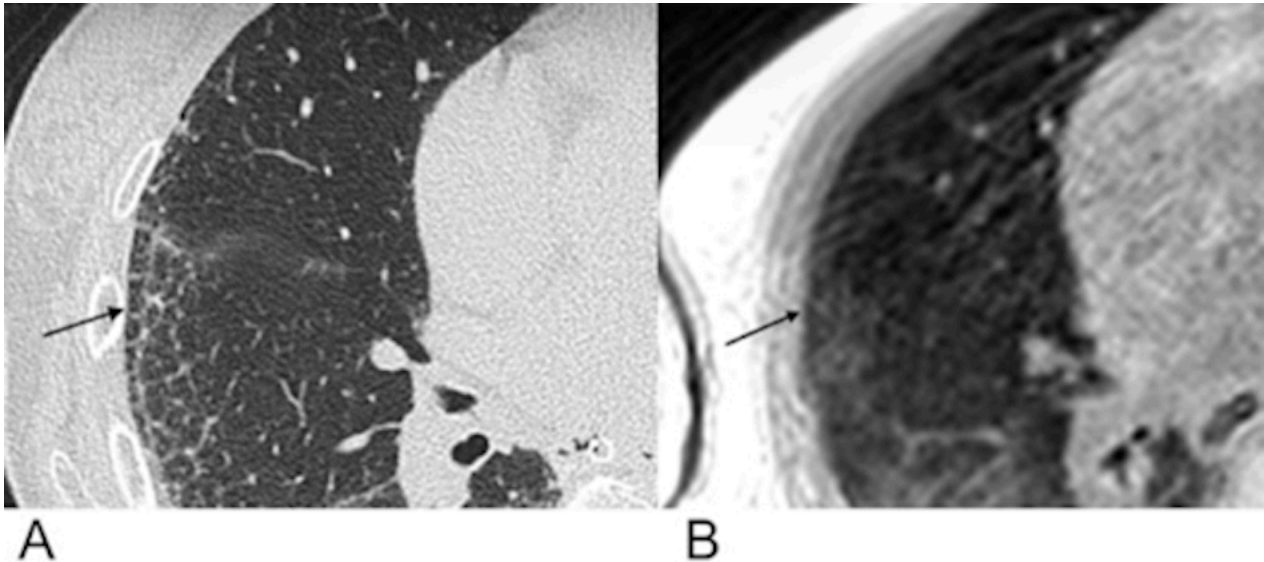


Fig. 4 SSc-ILD, particular of the right lung: UTE are less reliable in RET assessment.

On UTE (B) RET, that are easily recognizable on CT (A), may be misinterpreted because of partially collapsed alveoli in free breathing acquisition.

Legend

SSc: Systemic Sclerosis; CT: Computed Tomography; UTE: Ultrashort Echo Time Spiral VIBE MRI sequence; ILD: Interstitial Lung Disease; RET: reticulations

Moreover, we decide to test the feasibility of DCE-MRI analysis, as proposed by Yi et al., trying to identify pattern of prevalent inflammation, manifesting as an early enhancement pattern, or prevalent fibrosis, manifesting as a no-peak of enhancement or a delayed enhancement. The contrast evaluations demonstrated good intra- and inter-reader agreements, proving to be feasible, even if a few patients accepted to perform DCE-MRI, maybe for the length of the entire protocol. One chance could be perform only DCE-MRI in patients with ascertained ILD, with the only purpose of adding functional data on morphologic CT evaluation. However, our preliminary results suggested that fibrosis is quite always present in SSc-ILD (Figure 5), while predominant inflammatory ILD are uncommon. Considerations on the effects of therapy were out of the aim of this work and we did not correlated the MRI findings with therapeutic status. However, we could hypothesize that the immunosuppressive therapy may reduce inflammatory components of ILD but, on the other hand, that ILD alterations may rapidly turn into fibrotic alterations. This is in line with the recent attempts to test antifibrotic drugs, that are accepted as the main therapy in idiopathic pulmonary fibrosis, also for secondary ILD⁴⁹, assuming that a fibrotic component may be one more therapeutic target. Thus, we confirm a potential role of MRI in providing additional that may support the therapeutic strategy in SSc-ILD.

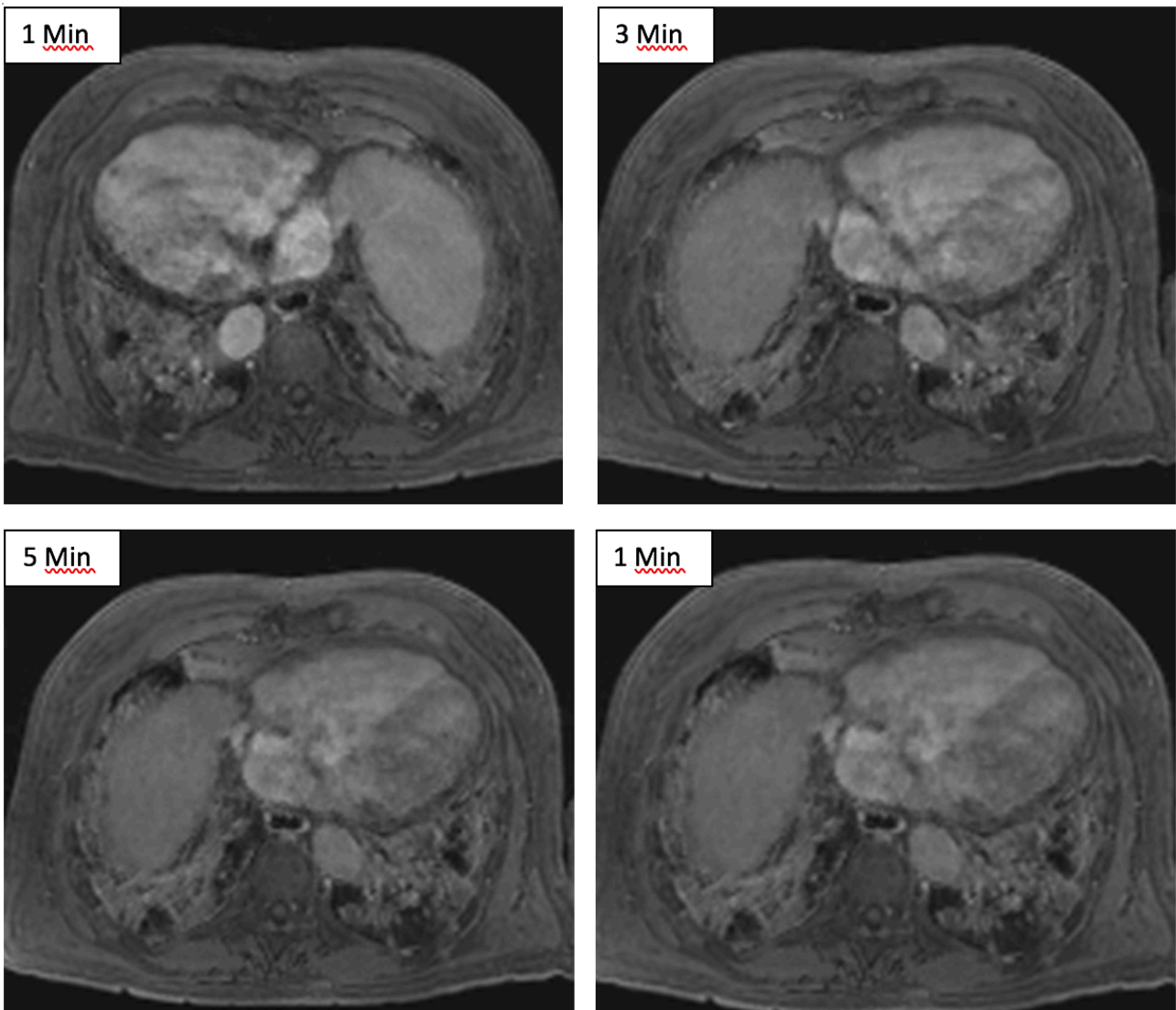


Fig. 5 SSc-ILD, DCE-MRI, VIBE contrast enhancement evaluation (1, 3, 5 and 10 minutes after contrast administration): delayed enhancement.

Images acquired 1, 3, 5 and 10 minutes after contrast administration did not show any peak of enhancement in ILD alterations. This pattern is consistent with a delayed enhancement, related to the presence of fibrosis.

Legend

SSc: Systemic Sclerosis; VIBE: Volumetric Interpolated Breath-hold Examinations; ILD: Interstitial Lung Disease;

RET: reticulations

Strengths of our study included the same-day acquisition of CT and MRI, as well as the CT QA analysis.

However, we have to acknowledge some limits. Firstly, anatomical levels for sQA could have slightly

differed between full inspiration on CT and free breathing scans on UTE. However, sQA performed in the current study is a sampling method that should be representative of the whole lung parenchyma⁵⁰, and small differences in anatomical levels (figure 2) should not be so relevant in quantifying a diffuse lung disease such as SSc-ILD. Moreover, we tested UTE also against CT QA, that is a whole lung parenchyma evaluation, and we obtained similar results than against CT sQA. To avoid the possible levels mismatch in sQA, one solution could have been a whole lungs visual evaluation for both CT and UTE. However, among visual ILD scoring systems that are usually considered for SSc, if the whole parenchyma is evaluated by the analysis of each lobe, the total score is based on wider ranges of involvement percentage (i.e. assigning one point for each 25%, per each lobe)⁵⁰: this scoring system, in our opinion, may result in a more approximated quantification. On the other hand, assessing the whole lobes to the nearest 5% of involvement would be really challenging and scarcely feasible in a clinical setting. Secondly, the low extent of HC on CT images made difficult to assess the full diagnostic potential of UTE for this kind of alterations, being HC less common than GGO combined with RET in SSc-ILD³. Lastly, the small amount of patients with ILD and contrast administration did not allow to extrapolate data that may allows general considerations on the prevalence of inflammation and/or fibrosis in SSc-ILD population.

5. CONCLUSIONS

The respiratory triggered Spiral VIBE MRI sequence is a reliable imaging tool in ILD and GGO extents analysis in SSc-ILD patients, although it may suffer of a low inter-reader agreement in mild ILD diagnosis. On the other hand, RET extent assessment remains challenging for this MRI sequence. A dynamic CE MRI analysis is feasible and could add information on inflammatory ILD activity.

REFERENCES

1. Tansey D, Wells AU, Colby T V, et al. Variations in histological patterns of interstitial pneumonia between connective tissue disorders and their relationship to prognosis. *Histopathology*. 2004;44:585-596.
2. Atzeni F, Gerardi MC, Barilaro G, Francesco I, Benucci M, Sarzi-Puttini P. Interstitial lung disease in systemic autoimmune rheumatic diseases: a comprehensive review. *Expert Rev Clin Immunol*. 2018;14(1):69-82. doi:10.1080/1744666X.2018.1411190.
3. Kim EA, Lee KS, Jonkoh T, et al. Interstitial Lung Diseases Associated with Collagen Vascular Diseases: Radiologic and Histopathologic. *Radiographics*. 2002;22:151-165.
4. Ohno Y, Koyama H, Yoshikawa T, Seki S. State-of-the-Art Imaging of the Lung for Connective Tissue Disease (CTD). *Curr Rheumatol Rep*. 2015;17(12):69. doi:10.1007/s11926-015-0546-8.
5. Capobianco J, Grimberg A, Thompson BM, et al. Thoracic manifestations of collagen vascular diseases. *Radiographics*. 2012 Jan-Feb;32(1):33-50. doi: 10.1148/rg.321105058.
6. Hansell DM, Bankier AA, MacMahon H, McLoud TC, Müller NL, Remy J. Fleischner Society: Glossary of Terms for Thoracic Imaging. *Radiology*. 2008;246(3):697-722. doi:10.1148/radiol.2462070712
7. Taouli B, Brauner MW, Mourey I, Lemouchi D, Grenier PA. Thin-section chest CT findings of primary Sjögren's syndrome: Correlation with pulmonary function. *Eur Radiol*. 2002;12(6):1504-1511. doi:10.1007/s00330-001-1236-7.
8. Wells AU, Denton CP. Interstitial lung disease in connective tissue disease — mechanisms and management. *Nat Publ Gr*. 2014;10(12):728-739. doi:10.1038/nrrheum.2014.149.

9. Winstone TA, Assayag D, Wilcox PG, et al. Predictors of mortality and progression in scleroderma-associated interstitial lung disease: A systematic review. *Chest*. 2014;146(2):422-436. doi:10.1378/chest.13-2626.
10. Cipriani NA, Streck M, Noth I, et al. Pathologic Quantification of Connective Tissue Disease – Associated Versus Idiopathic Usual Interstitial Pneumonia. *Arch Pathol Lab Med*. 2012;136:1253–1258. doi:10.5858/arpa.2012-0102-OA.
11. Bryson T, Sundaram B, Khanna D, Kazerooni EA. Connective Tissue Disease – Associated Interstitial Pneumonia and Idiopathic Interstitial Pneumonia: Similarity and Difference. *Semin Ultrasound, CT, MRI*. 2014;35(1):29-38. doi:10.1053/j.sult.2013.10.010.
12. Lutterbey G, Groh C, Gieseke J, et al. Initial experience with lung-MRI at 3.0 T: Comparison with CT and clinical data in the evaluation of interstitial lung disease activity. *Eur J Radiol*. 2007;61:256-261. doi:10.1016/j.ejrad.2006.09.005
13. Launay D, Remy-Jardin M, Michon-Pasturel U et al. High resolution computed tomography in fibrosing alveolitis associated with systemic sclerosis. *J Rheumatol* 2006;33:1789-1801.
14. Kim HJ, Tashkin DP, Gjerston DW, et al. Transitions to different patterns of interstitial lung disease in scleroderma with and without treatment. *Ann Rheum Dis*. 2016;75:1367-1371. doi:10.1136/annrheumdis-2015-208929.
15. Cottin V, Hirani NA, Hotchkin DL, et al. Presentation, diagnosis and clinical course of the spectrum of progressive-fibrosing interstitial lung diseases. *Eur Respir Rev*. 2018;27(150):180076. doi:10.1183/16000617.0076-2018
16. Ciet P. MRI in interstitial lung disease (M-ILD): a momentum to innovate lung diagnostic. *Thorax*. 2021;76(2):108-108. doi:10.1136/thoraxjnl-2020-216382

17. Romei C, Turturici L, Tavanti L et al. The use of chest magnetic resonance imaging in interstitial lung disease: a systematic review. *Eur Respir Rev* 2018;27:180062.
18. Wild JM, Marshall H, Bock M, et al. MRI of the lung (1/3): methods. *Insights Imaging*. 2012;3: 345–53.
19. Ohno Y, Nishio M, Koyama H, et al. Pulmonary MR imaging with ultra-short TEs: utility for disease severity assessment of connective tissue disease patients. *Eur J Radiol* 2013; 82: 1359–1365.
20. Dournes G, Grodzki D, Macey J, et al. Quiet Submillimeter MR imaging of the lung is feasible with a PETRA sequence at 1.5 T. *Radiology* 2015; 276: 258–265.
21. Ohno Y, Chen Q, Hatabu H. Oxygen-enhanced magnetic resonance ventilation imaging of lung. *Eur J Radiol* 2001; 37: 164–171.
22. Ohno Y, Hatabu H, Takenaka D, et al. Dynamic oxygen-enhanced MRI reflects diffusing capacity of the lung. *Magn Reson Med* 2002; 47: 1139–1144.
23. Triphan SM, Breuer FA, Gensler D, et al. Oxygen enhanced lung MRI by simultaneous measurement of T1 and T2 * during free breathing using ultrashort TE. *J Magn Reson Imaging* 2015; 41: 1708–1714.
24. Molinari F, Eichinger M, Risse F, et al. Navigator-triggered oxygen-enhanced MRI with simultaneous cardiac and respiratory synchronization for the assessment of interstitial lung disease. *J Magn Reson Imaging* 2007; 26: 1523–1529.
25. Ohno Y, Nishio M, Koyama H, et al. Oxygen-enhanced MRI for patients with connective tissue diseases: comparison with thin-section CT of capability for pulmonary functional and disease severity assessment. *Eur J Radiol* 2014; 83: 391–397.
26. Stadler A, Jakob PM, Griswold M, et al. T1 mapping of the entire lung parenchyma: influence of the respiratory phase in healthy individuals. *J Magn Reson Imaging* 2005; 21: 759–764.

27. Stadler A, Jakob PM, Griswold M, et al. T1 mapping of the entire lung parenchyma: influence of respiratory phase and correlation to lung function test results in patients with diffuse lung disease. *Magn Reson Med* 2008; 59: 96–101.
28. Lutterbey G, Grohé C, Gieseke J, et al. Initial experience with lung-MRI at 3.0T: comparison with CT and clinical data in the evaluation of interstitial lung disease activity. *Eur J Radiol* 2007; 61: 256–261.
29. Yi CA, Lee KS, Han J, et al. 3-T MRI for differentiating inflammation- and fibrosis-predominant lesions of usual and nonspecific interstitial pneumonia: comparison study with pathologic correlation. *AJR Am J Roentgenol* 2008; 190: 878–885.
30. Buzan MT, Eichinger M, Kreuter M, et al. T2 mapping of CT remodelling patterns in interstitial lung disease. *Eur Radiol* 2015; 25: 3167–3174.
31. Benlala I, Albat A, Blanchard E, et al. Quantification of MRI T2 Interstitial Lung Disease Signal-Intensity Volume in Idiopathic Pulmonary Fibrosis: A Pilot Study. *J Magn Reson Imaging*. 2021;53(5):1500-1507. doi:10.1002/jmri.27454
32. Gaeta M, Blandino A, Scribano E, et al. Chronic infiltrative lung diseases: value of gadolinium-enhanced MRI in the evaluation of disease activity – early report. *Chest* 2000; 117: 1173–1178.
33. Marinelli JP, Levin DL, Vassallo R, et al. Quantitative assessment of lung stiffness in patients with interstitial lung disease using MR elastography. *J Magn Reson Imaging* 2017; 46: 365–374.
34. van den Hoogen F, Khanna D, Fransen J et al. 2013 classification criteria for systemic sclerosis: An American college of rheumatology/European league against rheumatism collaborative initiative. *Ann Rheum Dis*. 2013;72:1747-1755.

35. Sundaram B, Chughtai AR, Kazerooni EA. Multidetector high-resolution computed tomography of the lungs: protocols and applications. *J Thorac Imaging*. 2010;25(2):125-41.
36. Bae K, Jeon KN, Hwang MJ et al. Comparison of lung imaging using three-dimensional ultrashort echo time and zero echo time sequences: preliminary study. *Eur Radiol*. 2019;29(5):2253-2262
37. Occhipinti M, Bosello S, Sisti LG, Cicchetti G, de Waure C, Pirroni T, et al. Quantitative and semi-quantitative computed tomography analysis of interstitial lung disease associated with systemic sclerosis: A longitudinal evaluation of pulmonary parenchyma and vessels. *PLoS One*. 2019;12;14(3):e0213444.
38. Goh NS, Desai SR, Veeraraghavan S, Hansell DM, Copley SJ, Maher TM, et al. Interstitial lung disease in systemic sclerosis: a simple staging system. *Am J Respir Crit Care Med*. 2008;177:1248-1254.
39. McHugh ML. Interrater reliability: the kappa statistic. *Biochem Med (Zagreb)*. 2012;22(3):276-282.
40. Parikh R, Mathai A, Parikh S, Sekhar GC, Thomas R. Understanding and using sensitivity, specificity and predictive values. *Indian J Ophthalmology*. 2008;56:45-50.
41. Lin LI-K. A Concordance Correlation Coefficient to Evaluate Reproducibility. *Biometrics*. 1989;45:255-268.
42. Weatherley ND, Eaden JA, Stewart NJ et al. Experimental and quantitative imaging techniques in interstitial lung disease. *Thorax*. 2019;74(6):611-619.

43. Pinal-Fernandez I, Pineda-Sanchez V, Pallisa-Nuñez E Et al. Fast 1.5 T chest MRI for the assessment of interstitial lung disease extent secondary to systemic sclerosis. *Clin Rheumatol*. 2016;35:2339-2345.
44. Dournes G, Yazbek J, Benhassen W et al. 3D ultrashort echo time MRI of the lung using stack-of-spirals and spherical k-Space coverages: Evaluation in healthy volunteers and parenchymal diseases. *J Magn Reson Imaging*. 2018;48:1489-1497.
45. Ohno Y, Koyama H, Yoshikawa T Et al. Pulmonary high-resolution ultrashort TE MR imaging: Comparison with thin-section standard- and low-dose computed tomography for the assessment of pulmonary parenchyma diseases. *J Magn Reson Imaging*. 2016;43:512-532.
46. Perelas A, Silver RM, Arrossi AV, Highland KB. Systemic sclerosis-associated interstitial lung disease. *Lancet Respir Med*. 2020;8:304-320.
47. Veldhoen S, Heidenreich JF, Metz C et al. Three-dimensional Ultrashort Echotime Magnetic Resonance Imaging for Combined Morphologic and Ventilation Imaging in Pediatric Patients with Pulmonary Disease. *J Thorac Imaging*. 2021; 36:43-51.
48. Kuo W, Ciet P, Tiddens HA, Zhang W, Guillerman RP, van Straten M. Monitoring cystic fibrosis lung disease by computed tomography. Radiation risk in perspective. *Am J Respir Crit Care Med*. 2014;189:1328-1336.
49. Johannson KA, Chaudhuri N, Adegunsoye A, Wolters PJ. Treatment of fibrotic interstitial lung disease: current approaches and future directions. *The Lancet*. doi:10.1016/S0140-6736(21)01826-2

50. Assayag D, Kaduri S, Hudson M, Hirsch A and Baron M. High Resolution Computed Tomography Scoring Systems for Evaluating Interstitial Lung Disease in Systemic Sclerosis Patients. *Rheumatology*. 2012;S1-003